



Purcell enhancement using spatially distributed random cavities enabled by silicon pyramid arraysMegha Khokhar,^{1,*} Nitesh Singh ^{1,*} Shinki,² Subhendu Sarkar,² and Rajesh V. Nair ^{1,†}¹Laboratory for Nano-scale Optics and Meta-materials (LaNOM), Department of Physics, Indian Institute of Technology Ropar, Punjab 140001, India²Surface Modification and Applications Laboratory (SMAL), Department of Physics, Indian Institute of Technology Ropar, Punjab 140001, India

(Received 2 December 2023; revised 6 July 2024; accepted 29 July 2024; published 23 August 2024)

The tailored disorder explores light-matter interaction with various functionalities in solar photovoltaic, lasing, structural coloration, and quantum technologies. However, studies are limited to exploring tailored disorder-induced light scattering, while the interactions between emitters and random cavities still need to be analyzed. We demonstrate a significant Purcell-enhanced emission using random cavities in a spatially dispersed silicon (Si) pyramid array. The numerical simulation reveals spatial confinement of electric field intensity in the cavity with substantial Purcell enhancement for an embedded emitter. We experimentally verify Purcell enhancement using localized emitters coupled to Si pyramids, demonstrating fivefold enhanced emission intensity. We achieve a 67% reduction in emission lifetime for random cavity-coupled emitters, which depends on Si pyramid density across the sample, supported with numerical simulations. Our results put forward an amenable approach to tailoring random cavities to manipulate the emission properties of quantum emitters.

DOI: [10.1103/PhysRevA.110.023522](https://doi.org/10.1103/PhysRevA.110.023522)**I. INTRODUCTION**

Controlling emission dynamics of light emitters has become a backbone of modern atomic and optical physics that led to insights in sensing, lasing, plasmonics, and solar photovoltaics [1–6]. Enabling emitter coupling using cavities is required to achieve emission enhancement, directionality, strong-coupling regime, low-threshold lasing, and on-demand single photon generation [7,8]. This is possible due to the enhanced local density of optical states (LDOS), which controls light-matter interaction of the emitters placed in the cavity through Fermi’s “golden rule” [9,10]. Photonic crystal cavities are the champion structures that allow controlled classical and quantum applications by engineering ordered photonic structures. Such ordered structures are tailored by varying geometry to have precise control for applications [7,8,11–19]. However, the photonic or plasmonic cavity structures are sensitive to inherent sample imperfections and finite-size effects [20–23]. This has shifted the interest in exploring structures with intentional or unintentional disorder that allow localization of emitted light and thus enhance emission [24,25].

The LDOS enhancement using cavities is defined using the Purcell factor that depends on the spatial and spectral overlap between the cavity mode and emitter emission profile [6,7]. Usually, Purcell enhancement is used to describe emission rate modification, defined as the ratio between emission rate of an emitter placed in a cavity and emission rate in a homogeneous medium. Spatially correlated disordered photonic structures are explored for tuning LDOS to manipulate light transport

and emission [26–32]. Photonic crystal waveguides with tailored disorder have been used to achieve Purcell enhancement by exciting localized modes with promising applications compared to their complementary ordered structures [24,27,32]. This includes applications such as random lasing, light trapping, antireflection, and LDOS tuning [26,33–35]. However, these waveguides require rigorous tuning to couple emitters with disordered cavities. It also requires complex fabrication protocols and low-temperature operation to activate embedded emitters [27].

Recently, two-dimensional (2D) random arrays of micron-sized silicon (Si) pyramids have attracted attention due to their excellent light trapping capabilities, ease of fabrication, scalability, and as a substrate for Raman enhancement [36–42]. They are effectively utilized in ultrathin solar cells to improve cell efficiency through photon absorption enhancement and to tune magnetic properties of materials [43–45]. The Si pyramid structure is also proposed as a broadband omnidirectional antireflector and an antibacterial surface [46–48]. These previously reported studies are primarily concerned with applications related to design parameters or structural aspects of Si pyramids. It is shown that the textured Si surfaces can enhance photonic DOS, leading to an intensity enhancement effect through field confinement that allows for absorption [49]. It suggests that the light can directly couple from incident medium to Si pyramid structure. In the time reversal process, when emitters are coupled with such structures, the emitted light can effectively decouple from the structure and are emitted out. Thus, a properly tuned Si pyramid structure can host random cavities, which could be a platform for achieving Purcell enhancement for a coupled emitter. However, it is not universally true when the system induces nonradiative decay channels or when the quantum efficiency of the emitter is significantly low. In such cases,

*These authors contributed equally to the work.

†Contact author: rvnair@iitrpr.ac.in

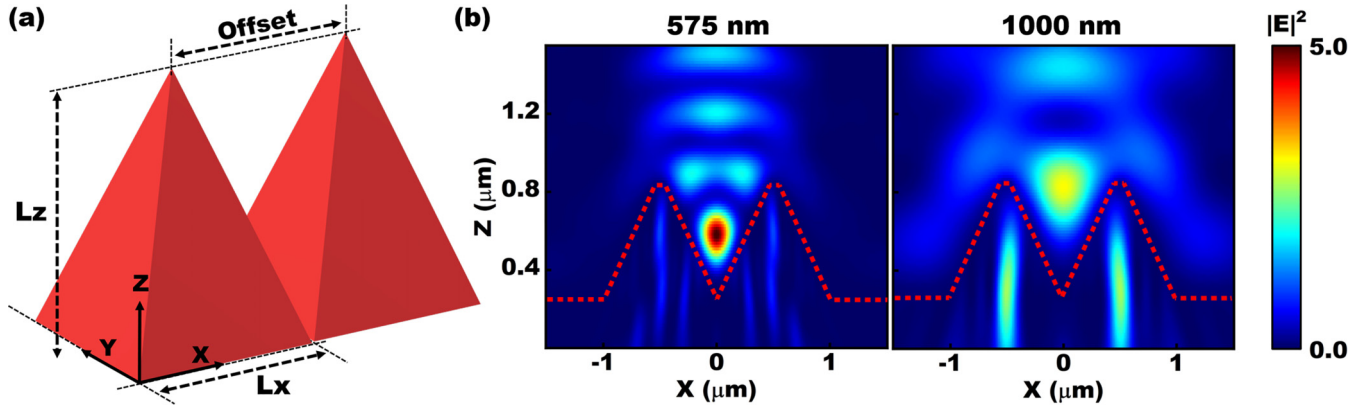


FIG. 1. (a) Two parallel-facing Si pyramids having L_z and L_x as height and base width, respectively. An offset value gives distance between two pyramids' center. (b) Electric field intensity confinement is obtained near the bottom of pyramids' valley at 575 nm, while confinement is minimal for 1000 nm incident light and occurs near the top of pyramids. Red dotted lines show the pyramid's outer edge.

the nonradiative component will affect the system, resulting in quenching of the emission.

In contrast, earlier studies have concentrated on investigating design parameters of Si pyramids to achieve antireflection coatings and a platform to enhance absorption for incident light. However, coupling the emitter to the random arrays of Si pyramids has not yet been explored. Such coupling enables control over emission properties of coupled emitters with significant enhancement in emission, which provides a path to innovative applications. In addition to emission rate enhancement, the directionality of emitted light can be improved using random cavities. Such easy-to-fabricate random cavities induce a paradigm shift in enhancing emission rate of localized emitters with applications in classical and quantum photonic technologies [3,15–17,22,27].

Here, we report Purcell enhancement with improved emission collection and directionality from dye molecules coupled to random cavities created using a 2D array of Si pyramids. The random cavities are simulated by randomizing the base and height of Si pyramids using the finite difference time domain (FDTD) method to understand the extent of spatial light confinement. The fabricated random cavities are coupled with dye molecules to experimentally study the Purcell enhancement and their spatial variation across the sample. The time-resolved and photoluminescence emission measurements show the Purcell enhancement for emitters coupled with such random cavities, supported by simulations. The spatial-dependent fluctuations in emission rate are observed owing to pyramid density variations across sample.

II. RESULTS AND DISCUSSION

A. Cavity design using two pyramids

We consider the cavity formed using two parallel placed Si pyramids, as shown in Fig. 1(a). The Si pyramids are designed using an inbuilt script programming language available with the FDTD method (Ansys, Lumerical). The wavelength-dependent Si refractive index is taken from the Palik handbook for calculations [50] (see Supplemental Material I, Fig. S1a [51]). The configuration of two pyramids

significantly reduces computational time. The pyramids are positioned on a Si substrate in the x - y plane with height (L_z) and base width (L_x). The separation between pyramids is given by an offset value derived from pyramid's center, as shown in Fig. 1(a). The sample region used for FDTD calculations is $3 \mu\text{m} \times 2 \mu\text{m}$ wide in the x and y directions and $2.2 \mu\text{m}$ wide along the z direction with a perfectly matching layer as the boundary. We impinge a Gaussian beam of wavelength 575 and 1000 nm on Si pyramids, and electric field intensity between pyramids is calculated using a frequency-domain profiler and power monitor placed in the x - z plane. The optimized $L_z = 600$ nm and $L_x = 1000$ nm are used to achieve maximum field intensity confinement between pyramids at 575 nm. However, a minimal value of L_z and L_x is essential to maintain light confinement within the pyramids' valley (Supplemental Material I, Fig. S2). The distance between pyramids varies from top to bottom, with maximum and minimum spacing at top and bottom, respectively. The incident light is trapped in cavity by recurrent reflections between pyramid faces, leading to resonant mode formation that can confine light intensity between pyramids [52]. Optimizing geometry and material properties of the pyramid enables broad wavelength light confinement, which is helpful for various applications [53].

Figure 1(b) shows the cross-sectional view of light confinement in the cavity region between two pyramids (dotted red line) for 575 and 1000 nm incident light. The L_x and L_z values are optimized for maximum field confinement for 575 nm. We observe a substantial confinement for 575 nm compared to 1000 nm. The location of high-intensity regions in the cavity also differs for both wavelengths. The intensity corresponding to 575 nm is localized precisely at the center between pyramids, whereas 1000 nm light is reflected back into incident medium. The pyramid parameters are varied to optimize sample for maximum field confinement between pyramids (Supplemental Material I, Fig. S2 and Table S1 [51]). The field confinement region can be modulated using an offset value, defining separation between pyramids. It is found that maximum field confinement region shifts downside towards the substrate with an increase in offset value (Supplemental Material I, Fig. S3). The optimization of pyra-

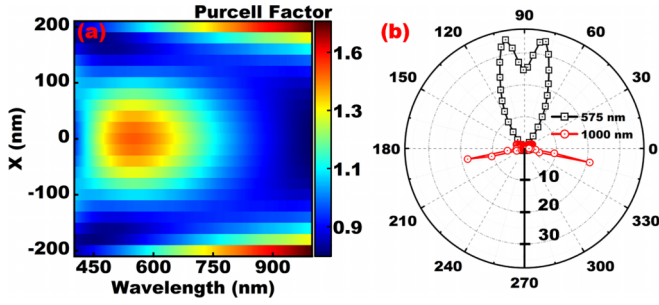


FIG. 2. (a) Purcell factor calculation for the 400–1000-nm spectral range at various dipole locations along the x axis. The dipole is oriented horizontally with respect to the Si substrate and placed at a high-field confinement region between pyramids. Near $x = 0$ nm, the Purcell factor increases for wavelength 575 nm. (b) The far-field radiation enhancement from emitter placed at $x = 0$ nm in the two-pyramid configuration.

mid parameters is helpful to realize cavity-coupled emitters to achieve emission enhancement.

B. Purcell enhancement and far-field radiation

The Purcell factor is calculated to understand the extent of field confinement inside the cavity to increase emission rate of an embedded emitter. The Purcell effect is a collective consequence of field confinement within cavity and increased LDOS. According to Fermi's golden rule, spontaneous emission rate (γ) depends on available density of optical states (DOS) at emission wavelength: $\gamma = \frac{2\pi}{\hbar} \sum_f |\langle f | \hat{H}_I | i \rangle|^2 \delta(\omega_f - \omega_i)$, where $\hat{H}_I = -\hat{\mu} \cdot \hat{E}$ is the interaction Hamiltonian in dipole approximation with the dipole moment operator ($\hat{\mu}$) and field operator (\hat{E}). If emission is sensitive to local environment, then LDOS is a more relevant quantity to calculate local environment-dependent emission rate (γ_l) [54]. The γ_l is related to LDOS in terms of Green's function (\vec{G}): $\gamma_l = \frac{2\omega_o}{3\hbar\epsilon_o} |\vec{\mu}|^2 \rho_l(\vec{r}_o, \omega_o)$, where $\rho_l(\vec{r}_o, \omega_o) = \frac{6\omega_o}{\pi c^2} \text{Im}\{\hat{n} \cdot \vec{G}(\vec{r}_o, \vec{r}_o; \omega_o) \cdot \hat{n}\}$ is the LDOS for a given dipole orientation within the system with unit vector \hat{n} in the direction of dipole moment $\vec{\mu}$. The resulting electric field at a location (\vec{r}) radiated by dipole (oriented along a given axis) located at \vec{r}_o computes the component of Green's dyadic \vec{G} [54]. In general, for all three orthogonal dipole orientations, the electric field and \vec{G} are related as

$$\vec{E}(\vec{r}) = \frac{\omega^2 \mu_o \mu_r}{n^2} \vec{G}(\vec{r}, \vec{r}_o) \cdot \vec{\mu}, \quad (1)$$

where each diagonal element of \vec{G} (G_{xx} , G_{yy} , G_{zz}) corresponds to the electric field component of the dipole oriented along the x , y , and z axes (E_x , E_y , E_z).

The ratio of γ_l when the emitter is in a cavity to the emitter in a free space, provides a Purcell factor, which is directly proportional to LDOS. A high Purcell factor indicates that the emission rate is enhanced due to an increased LDOS within the cavity [55]. Figure 2(a) shows a spectral-dependent Purcell factor for a dipole placed between the region of two pyramids. The calculations are done at various x positions

for $y = 0$ nm and $z = 570$ nm as it contains regions of both high and low electric field intensity distribution. The \vec{G} is calculated by considering different dipole orientations for Purcell factor calculations. However, it is observed that a dipole with orientation parallel to the pyramid face (along the y axis) shows a maximum Purcell factor at 575 nm. Thus, the calculations proceed further only with a dipole having orientation parallel to the pyramid face. The calculated Purcell factor shows the maximum value for a dipole placed in the region of maximum field intensity at 575 nm, as seen in Fig. 1(b). The enhanced Purcell factor confirms a LDOS increase at a cavity's center ($x = 0$ nm) formed by pyramids, where maximum overlap between dipole moment and cavity mode is obtained. The Purcell factor is constant within $x = \pm 25$ nm between pyramids. Higher values are also observed near ± 200 nm from the pyramid center. Such higher values are because of absorption when the emitter is very close to the Si, which is due to the nonradiative part of the Purcell factor (Supplemental Material I, Fig. S1b). Figure 2(b) shows the calculated far-field radiation pattern for a dipole emitting at 575 and 1000 nm placed in a cavity compared to dipole emission above the Si substrate without pyramids. The radiation pattern emphasizes that the emission is directional for 575 nm emission wavelength (open black squares) compared to 1000 nm (open red circles). At 575 nm, the emission is directed towards the upward direction within $\pm 15^\circ$ due to the cavity effect induced by parallel placed Si pyramids. The calculations also show that the structure directs 30 times more emission towards the collection objective than the bare Si substrate. However, at 1000 nm, the emission is scattered sideways as it is not a cavity-optimized wavelength. This is also corroborated by the field calculations shown in Fig. 1(b), wherein the field at 1000 nm penetrates inside the pyramids. The near-field dipole emission intensity enhancement toward the positive z axis, improving the collection of emitted light (Supplemental Material I, Fig. S4). The results demonstrate the possibility to obtain the enhanced Purcell factor and emission collection using parallel placed Si pyramids. The Si pyramids are then randomized to study the formation of random cavities in a disordered array of Si pyramids.

C. Design and fabrication of random cavities

The random Si pyramid cavities are designed using script commands in Lumerical (Supplemental Material I). Figures 3(a)–3(d) show electric field intensity confinement between pyramids, arranged randomly with varying pyramids' density for 575 nm incident light. The intense buildup of field intensity is observed between pyramids, which arises due to trapped light in the presence of random cavities, increasing field intensity magnitude. Figure 3(a) shows a random distribution of six pyramids of different sizes. The pyramids are at a larger distance from each other, resulting in minimal field confinement. However, when pyramid density is increased, the field confinement regions and field intensity increase, as shown in Fig. 3(b). It is found that increasing pyramid density alone does not necessarily enhance field confinement; instead, it depends upon both the pyramid's size and density.

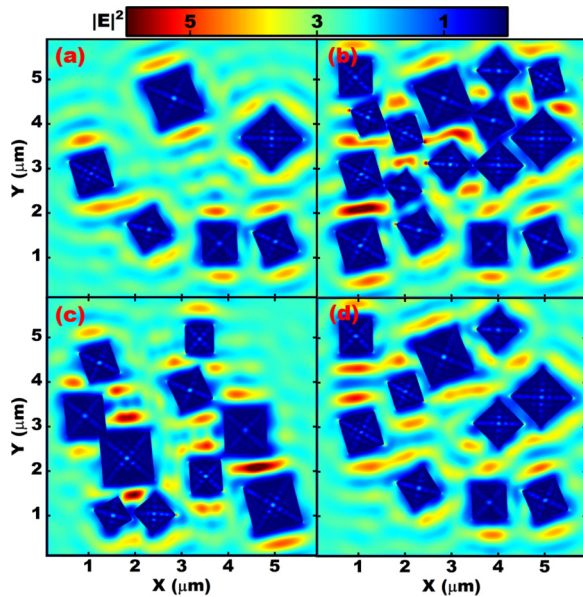


FIG. 3. Randomly distributed pyramid cavities (x - y view, 575 nm). (a) The six pyramids are relatively far from each other; hence, minimal light confinement is obtained between pyramids. (b) Sixteen random pyramids are added to configurations shown in (a), effectively inducing more light confinement between pyramids. (c), (d) The randomly rearranged ten pyramids show a change in spatial region of light confinement.

Figures 3(c) and 3(d) show the field intensity confinement due to random cavities created using ten pyramids. The pyramids are randomized to achieve different types of random cavity configurations. The absence of field intensity confinement for 1000 nm incident light confirms that the confinement depends on incident wavelength (Supplemental Material I, Fig. S5). Additionally, the upper and lower limits of structure parameters are taken to strengthen field confinement at 575 nm, which would not work efficiently for 1000 nm. The results indicate that the field intensity confinement obtained in the random cavities formed by Si pyramids can substantially modify the emission rate of an embedded emitter.

We have experimentally studied the emission dynamics of dye molecules [Rhodamine 6G (R6G), Sigma Aldrich] emitting at 575 nm coupled with an array of random Si pyramids to verify the simulation results. The Si pyramids are fabricated on Si substrate using the chemical etch method (Supplemental Material II [51]). Figure 4(a) shows the scanning electron microscope (SEM) image of the sample, depicting randomly positioned Si pyramids. The cross-sectional SEM image in Fig. 4(b) shows randomly arranged vertical pyramids facing each other, similar to geometry used in simulations. We find significant variation in base length from 0.5 to 9.5 μm with a maximum pyramid base size between 2 and 3 μm with an average height of 1.13 μm , similar to values used in simulation (Supplemental Material II, Fig. S6). The pyramids' density varies across the sample, which provides different field intensity confinement, as seen in Fig. 3, hence the spatial-dependent emission rate is expected. The Purcell enhancement induced by random cavities is studied by measuring emission intensity and rate of R6G dye molecules.

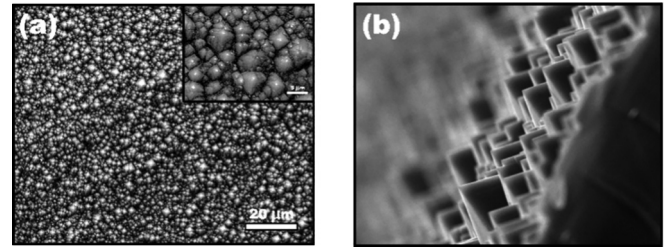


FIG. 4. (a) The SEM image of the sample, which depicts random formation of Si pyramids over a large area. The inset shows zoomed sample image with pyramids of varying geometrical parameters. (b) The cross-sectional SEM image of sample shows Si pyramids of different heights and bases.

D. Emission intensity and rate measurement: Purcell effect

Figure 5(a) shows a schematic of the sample with randomized Si pyramids drop casted with R6G dye molecules, excited using a 532-nm pulsed laser through a microscope objective of $20\times$ magnification with a 0.4 numerical aperture. The sample is scanned using a home-built confocal microscope to locate localized emitters trapped in random cavities (Supplemental Material III, Fig. S8 [51]). The emitted light is collected using the same objective in reflection geometry. Figure 5(b) shows a typical confocal image of a sample over a region of $0.75\ \mu\text{m}^2$ at 575 nm, which shows localized emission spots induced by the cavities. The bright region (red circle) shows emission from dye molecules coupled to a cavity formed due to Si pyramids. The dark region in the map represents a bare Si surface with some background emission intensity. There are also sample regions wherein the intensity is very low due to weak coupling of dye molecules with Si pyramids. A very high-intensity spot (yellow dotted circle) is also observed while mapping the sample. This region results from a scattering point on the pyramidal surface, confirmed by measuring the intensity for a longer duration and the time-resolved measurements. The emission intensity measurements are done by focusing on sample depth, which excites dye molecules trapped in cavity created by five to six randomly arranged pyramids. Figure 5(c) shows the measured emission intensity from dye molecule trapped between Si pyramids (red squares) and a reference sample (blue circles). We have taken R6G dye suspension as the reference sample. The band edge of long-pass dichroic mirror is noticeable in emission spectra of R6G with a cut-on wavelength at 550 nm, hence spectra appear slightly asymmetrical. The emission from R6G dye molecules drop-casted on a flat Si substrate (grey region) is lower due to emission quenching by the Si substrate. The measured emission spectra from Si pyramids show sixfold intensity enhancement compared to the reference sample at 575 nm. This emission intensity enhancement from the R6G dye molecule trapped between Si pyramids is due to the random cavity effect. The in-plane emission from the dye molecule undergoes recurrent reflection due to parallel facing Si pyramids like a Fabry-Perot cavity. The enhanced emission intensity from Si pyramid coupled dye molecules confirms that absorption is negligible compared to emission from flat Si substrate. The randomness is observed in terms of variation in pyramids' shape, size, and density over a given sample region.

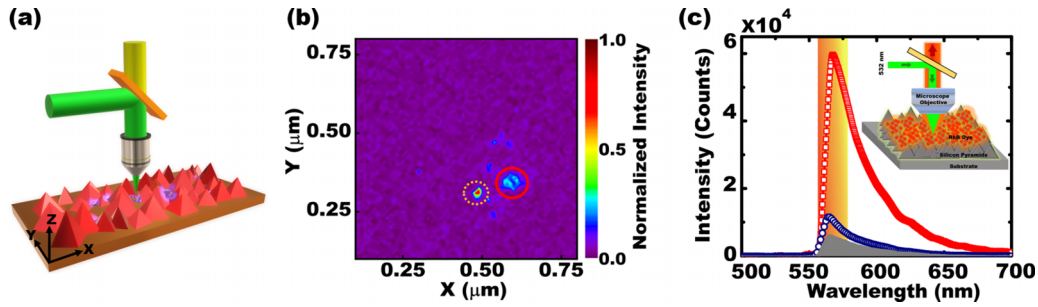


FIG. 5. (a) The schematic of random cavities formed using Si pyramids drop-casted with dye molecules, which are excited using 532 nm through $20\times$ microscope objective. (b) A confocal image is obtained from sample, which is spatially scanned in x - y directions over a region of $0.56\ \mu\text{m}^2$. (c) The emission intensity spectra acquired from sample (red squares) show enhanced emission intensity compared to R6G dye suspension (blue circles) and R6G dye on a flat Si substrate (grey region).

The cavity effect is observed when the system is studied on a scale of individual pyramids, such as a system of two pyramids separated by a definite distance. The observed Q factor is indeed lower than 10, forming a broad cavity mode. Thus, it is concluded that the random cavities show resonance behavior on a very local basis. Additionally, the cavity is an open-end structure with emitted light collected through the structure's top. Hence, emission or absorption in that direction is negligible, and out-of-plane emission is eventually collected by microscope objective in reflection geometry.

The enhanced emission intensity measurement corroborates localized field intensity between pyramids, as seen in Fig. 3. The confined field intensity within the sample couples with dipole emission and enhances emission due to the cavity effect. The improved emission collected by objective results from enhanced far-field radiation induced by cavity, similar to simulated results shown in Fig. 2(b). The geometry of pyramids increases the probability of light interaction with emitters, thus enhancing emission. However, during drop-casting of dye molecules, it is possible to have a large number of emitters localized in some sample regions compared to others. This difference in emitter concentration could be a reason for an increase in emission intensity. Additionally, measured enhancement in emission intensity could be a convoluted result of enhancement in pump field, variation in photonic environment, and enhanced detection efficiency. Hence, relying solely on emission intensity measurements may not accurately confirm enhanced emission induced by random cavities. Thus, decay rate measurements are required to confirm observed intensity enhancement by random cavities.

We perform decay rate measurements to estimate emission rate enhancement of coupled dye molecules to random cavities. The spatial-dependent decay rate measurements are performed to calculate average lifetime values while spatially scanning a sample. Accordingly, the measured lifetime values from different sample regions with higher and lower pyramid densities are compared with the reference sample. Figure 6(a) shows measured decay curves from the reference sample (red squares) compared to decay curves obtained from the sample region with low (blue circles) and high (pink triangles) density of Si pyramids at 575 nm. The fast decay curve (solid green line) corresponds to a scattering point on a sample without any emission, which accounts for instrument response function. The measured decay rate from the Si pyramids sample is

relatively fast compared to the reference sample, with an extremely fast decay obtained from a densely packed pyramids region. This suggests a spatial-dependent decay rate, a signature of LDOS fluctuation across random cavity structures. Such LDOS fluctuation is a trademark of emitters embedded in disordered photonic structures with long tail statistics in emission decay rate [27]. This authenticates that the Purcell effect depends on pyramid density for random cavities.

The measured decay curve from a sample is fitted using a biexponential function (solid lines) due to fast and slow lifetime components constituting the decay process. However, the emission from the reference sample is fitted using a single exponential function (dotted line), as shown in Fig. 6(a). The estimated lifetime value for the reference sample is 3.73 ns, similar to the known lifetime value for R6G dye suspension [56]. The emission decay curve from the sample is fitted using $I(t) = A_1 e^{-t/\tau_1} + A_2 e^{-t/\tau_2}$, where A_1 and A_2 are the peak amplitudes and τ_1 and τ_2 are the emission lifetime for slow and fast decay components at a particular emission intensity I for time t . The cavity-coupled emission fitting with a biexponential decay function confirms that additional decay channels are being offered due to cavity coupling. The average emission lifetime value $\langle\tau\rangle$ is obtained using $\langle\tau\rangle = \tau_1 \frac{A_1 \tau_1}{A_1 \tau_1 + A_2 \tau_2} + \tau_2 \frac{A_2 \tau_2}{A_1 \tau_1 + A_2 \tau_2}$ [57]. The estimated $\langle\tau\rangle$ value is 1.95 and 1.20 ns from sample regions with lower and higher

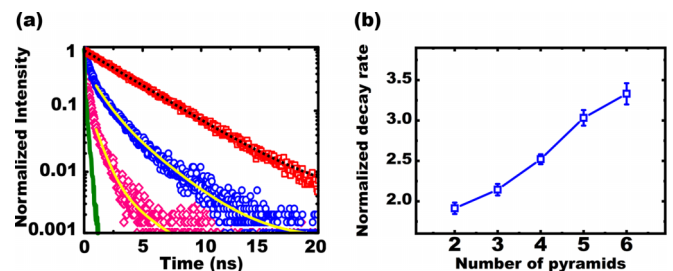


FIG. 6. (a) The decay curves of emission at 575 nm for the reference (red squares) and from low-density (blue circles) and high-density (pink triangles) pyramids on the sample with exponential fits (black dotted and yellow solid line). The green line indicates scattering from the sample. (b) The variation in Γ/Γ_0 values acquired across different regions on sample as a function of number of pyramids forming cavity. The overlaid lines emphasize the direction of the decay rate as number of pyramids increases.

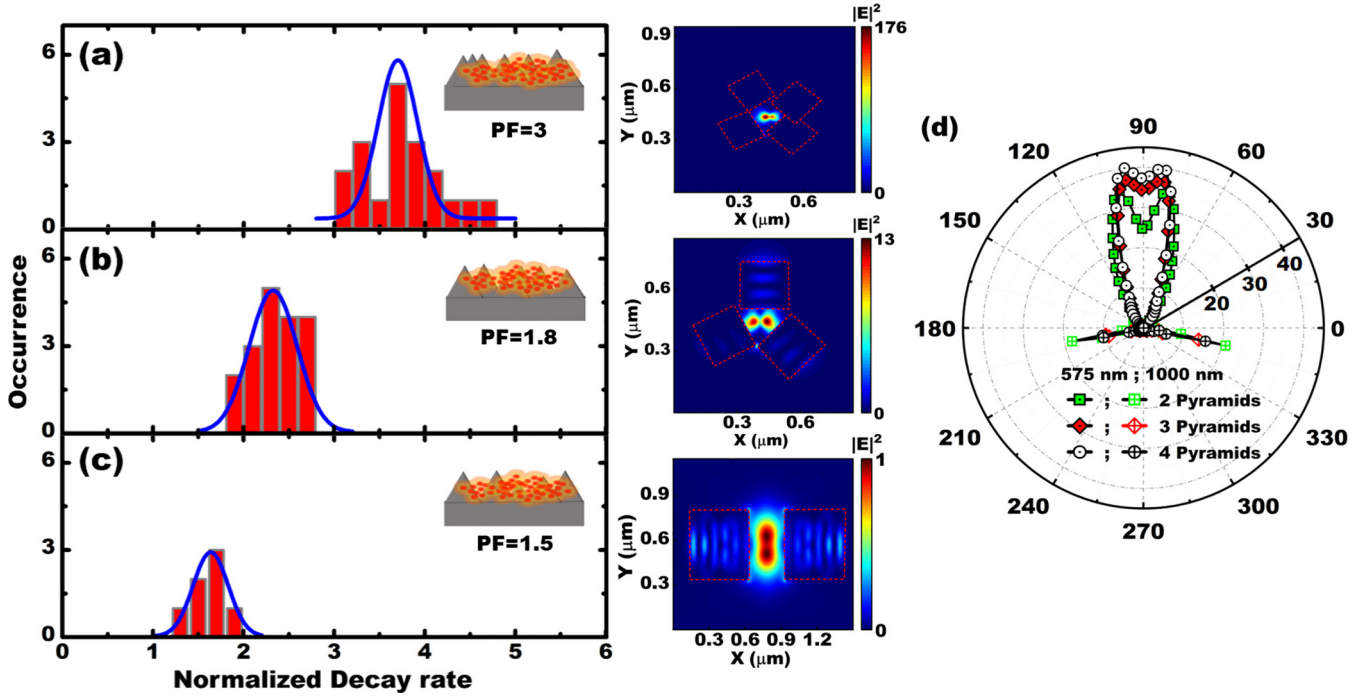


FIG. 7. The histograms (red bars) of the emission rate values are obtained from different spatial positions on sample with varying pyramid densities. (a) high dense pyramids region on sample, (b) less dense pyramids region on sample, and (c) least dense pyramids region on sample. The histograms are fitted with a Gaussian distribution function (solid blue line). Inset: The schematic of the pyramid density variation across sample with corresponding calculated Purcell factor (PF). The heat-map plots show the variation in field intensity confinement with variation in the density of pyramids. (d) The far-field radiation enhancement for different pyramid configurations.

density of Si pyramids, respectively. The strong reduction in lifetime corroborates increased LDOS due to stronger field intensity localization, as seen in the simulated result of Fig. 3(b). The decay rate measurements further confirm a substantial decrease in the $\langle\tau\rangle$ value from regions with high pyramid density compared to those with low density, suggesting density-dependent variation in emission rate and, thus, the LDOS fluctuations [35,58]. This fluctuation in emission rate is studied while scanning the whole sample with simultaneous imaging using a charge coupled device camera. The estimated lifetime from regions with very low pyramid density is similar to the lifetime value for the reference sample. The minimal field intensity confinement occurs when the pyramid density is low, as there are insufficient pyramids to support a strong cavity effect, similar to the simulation result in Fig. 3(a). We have also seen that when the excitation beam is positioned precisely between two pyramids, the lifetime value is estimated to be 1.14 ns due to a strong cavity effect. However, when the excitation beam is off-tuned from the cavity, the lifetime value increases as expected (Supplemental Material III, Fig. S9). Hence, it is essential to identify the right location on the sample to measure substantial Purcell enhancement induced by random cavity. The enhancement in collected emission intensity shown in Fig. 5(c), supported by decay rate enhancement, confirms radiative emission from cavity-coupled dye molecules. However, based on observed rates, the emitted light intensity surpasses the expected magnitude due to emission directivity induced by the pyramid cavity, as shown in Fig. 2(b). The measured values are comparable

to calculated values, which indicates that the dye molecules are situated between pyramids, supported by simulation results. The observation of the fast decay rate of coupled dye molecules with random cavities supports enhanced emission intensity.

E. Fluctuations in the measured decay rates

Figure 6(b) shows decay rate changes due to variations in Si pyramid density (number of pyramids) across the sample. The normalized decay rate (Γ/Γ_0) is acquired from the different regions of the sample, with Γ and Γ_0 being the decay rate of the sample and reference, respectively. We obtain the variation from $\Gamma/\Gamma_0 = 3.3$ for sample regions with high pyramids density to $\Gamma/\Gamma_0 = 1.9$ for sample regions with low pyramids density. The $\Gamma/\Gamma_0 = 1.9$ corresponds to $\langle\tau\rangle = 3.9$ ns from the sample region with low pyramid density, which conveys that dye emission is not affected by the sample. This implies that it is necessary to have sufficient pyramid density to induce a strong cavity effect that enables a strong Purcell effect. The results validate that the Purcell enhancement depends on pyramid density through better field intensity confinement, similar to simulation results. We perform spatial-dependent emission rate measurements in the sample to quantify spatial fluctuations in the emission rate. Figure 7(a) depicts the histogram of normalized decay rate (Γ/Γ_0) distribution obtained from the densely packed pyramids region. The distribution is fitted using the Gaussian function (solid blue line). As expected, the mean decay rate is quite high due to a strong Purcell

effect induced by the cavity, which depicts a strong coupling between emitted light and cavity mode. The mean value of Γ/Γ_0 distribution is 3.7 with a distribution width (w) of 0.51. Figures 7(b) and 7(c) represent the histogram of Γ/Γ_0 from the sample regions with low pyramid density. The mean value of the distributions is 2.37 with $w = 0.89$ and 1.67 with $w = 0.45$. We observe a large distribution width from sample regions with lower pyramid density compared to those with higher ones. This large width accounts for emission acquired from regions where dye molecules are not strongly coupled to random cavities, and most of the emission is collected from planar Si substrate.

Inset: Variation of average decay rate (in terms of Purcell factor) with pyramid density. The calculated Purcell factor for different pyramid densities agrees with measured values. The enhancement of electric field intensity for varying pyramid density is also shown. The higher pyramid density leads to stronger field confinement, resulting in a smaller mode volume and higher emission decay rate compared to samples with lower pyramid density. The formation of more complex clusters of pyramids leads to better light confinement (strong cavity effect). Panel (d) shows the normalized far-field radiation pattern for a dipole placed in cavity formed by two, three, and four pyramids emitting at 575 and 1000 nm. The far-field emission radiation pattern for 575 nm is enhanced towards the upward direction due to directionality induced by Si pyramids. Calculations show that the enhancement factor increases 40 times for higher pyramids density. The emission pattern for 1000 nm emitted light is scattered sideways as it is not the cavity-optimized wavelength. The Purcell factor values obtained are lower than those reported for photonic crystal cavities or plasmonic cavities [59,60]. The present work shows that the random arrangement of Si pyramids can significantly modify emission properties of coupled emitters by enhancing LDOS like an optical cavity. Naively, one may think that random arrangement induce multiple scattering in random directions without any type of localization and strong disorder requires for localization effects. However, we have shown a system wherein random arrangements of Si pyramids can induce localization by forming random cavities, which is experimentally verified using dye molecules coupled to such cavities. This enhancement is due to unique optical environment created by Si pyramids, which influences the behavior of nearby emitters. The proposed samples could, in principle, provide a significant Purcell effect through proper randomness engineering.

Further, pyramid density changes emission enhancement, implying strong spatial confinement of field intensity supported by FDTD simulations. The results propose an amenable approach to tailor the emission rate of quantum emitters using an easy-to-fabricate random cavity on a Si wafer. The proposed light confinement using random cavities would be useful for low-threshold lasing, tailored emission from single quantum emitters like color centers, and nonlinear optical processes due to precise spatial confinement of field intensity, and further engineering may lead to Anderson localization in these systems. The Si pyramids can significantly lead to enhanced emission efficiency due to their advantage of tailoring the interaction of light and emitter by optimizing geometry and spatial distribution of pyramids. The creation

of random cavities on Si using wet etching is easy but at the expense of Si having finite absorption in the region of dye emission. However, the enhanced emission is compared with emitters on a Si substrate, so the etched nature of the cavity induces the net effect. The proposed emission enhancement can be extended to random cavities created using other materials with different emitters or etched arrays on Si optimized for the near-IR wavelength ranges. Additionally, the enhanced emission efficiency led by random Si pyramids is advantageous for tailoring the light-matter interaction by optimizing the geometry and spatial distribution of pyramids. The benefits of this system extend to various applications, including surface enhanced raman scattering, lasing, and nonlinear optics, all of which depend on field confinement provided by Si pyramids. It would be interesting to explore scattering and polarization control of light using a random array of Si pyramids.

III. CONCLUSIONS

We have studied Purcell enhancement induced by random cavities formed using parallel-facing Si pyramids. The FDTD simulation results confirm enhanced Purcell effect for a dipole placed at the gap between two pyramids due to strong field intensity confinement. The randomization of Si pyramids shows field intensity confinement between pyramids, which depends on pyramid density. The emission intensity measurements from localized regions of Si pyramids show a substantial increase in emission counts of embedded dye molecules. The in-plane emission is reflected back and forth between pyramids due to the cavity effect, which enhances out-of-plane emission intensity. The emission decay rate measurements confirm Purcell enhancement induced by random cavities created by Si pyramids, which vary with pyramid density across the sample, substantiated by simulation results. The calculations show that the structure improves emission directionality by 30 times towards the collection objective compared to bare Si substrate. The experiments validate the calculations with six times the emission enhancement for coupled dye molecules. The proposed monolithic structure can be prepared to the size of a Si wafer without any lithographic techniques that offer a spatial variation of cavity mode. The structure provides a platform to couple quantum emitters, such as defects in diamonds and hexagonal boron nitride. The Si pyramids can significantly enhance emission efficiency due to their advantage of tailoring light-matter interactions by optimizing the geometry and spatial distribution of pyramids.

The data that support the findings of this study are available from the corresponding author upon reasonable request.

ACKNOWLEDGMENTS

The authors acknowledge financial support from IIT Ropar, Department of Science and Technology (DST), DST-ICPS (DST/ICPS/QuST/Theme-2/2019/General), DST-SERB (Grant No. SB/SJF/2020-21/05), and a Swarnajayanti fellowship (DST/SJF/PSA-01/2019-20). N.S. thanks IIT Ropar for a Ph.D. fellowship.

The authors declare no conflict of interest.

- [1] Z. Qian, L. Shan, X. Zhang, Q. Liu, Y. Ma, Q. Gong, and Y. Gu, Spontaneous emission in micro- or nanophotonic structures, *Photonix* **2**, 21 (2021).
- [2] J. S. van der Burgt and E. C. Garnett, Nanophotonic emission control for improved photovoltaic efficiency, *ACS Photonics* **7**, 1589 (2020).
- [3] M. Pelton, Modified spontaneous emission in nanophotonic structures, *Nat. Photonics* **9**, 427 (2015).
- [4] X. Miao, L. Yan, Y. Wu, and P. Q. Liu, High-sensitivity nanophotonic sensors with passive trapping of analyte molecules in hot spots, *Light: Sci. Appl.* **10**, 5 (2021).
- [5] J. J. Baumberg, J. Aizpurua, M. H. Mikkelsen, and D. R. Smith, Extreme nanophotonics from ultrathin metallic gaps, *Nat. Mater.* **18**, 668 (2019).
- [6] A. E. Krasnok, A. P. Slobozhanyuk, C. R. Simovski, S. A. Tretyakov, A. N. Poddubny, A. E. Miroshnichenko, Y. S. Kivshar, and P. A. Belov, An antenna model for the Purcell effect, *Sci. Rep.* **5**, 12956 (2015).
- [7] D. Englund, I. Fushman, and J. Vuckovic, General recipe for designing photonic crystal cavities, *Opt. Express* **13**, 5961 (2005).
- [8] A. Lyasota, C. Jarlov, M. Nyman, A. Miranda, M. Calic, B. Dwir, A. Rudra, A. Shevchenko, and E. Kapon, Mode interference effect in optical emission of quantum dots in photonic crystal cavities, *Phys. Rev. X* **12**, 021042 (2022).
- [9] S. V. Gaponenko, *Introduction to Nanophotonics* (Cambridge University Press, Cambridge, UK, 2010).
- [10] Priya and R. V. Nair, Scaling the spatial fluctuation of spontaneous emission suppression in photonic crystals, *Opt. Lett.* **44**, 2811 (2019).
- [11] X. Lu, A. McClung, and K. Srinivasan, High-Q slow light and its localization in a photonic crystal microring, *Nat. Photonics* **16**, 66 (2022).
- [12] D. Zhao, R. E. F. Silva, C. Climent, J. Feist, A. I. Fernández-Domínguez, and F. J. García-Vidal, Impact of vibrational modes in the plasmonic Purcell effect of organic molecules, *ACS Photonics* **7**, 3369 (2020).
- [13] P. C. Wu, W.-L. Hsu, W. T. Chen, Y.-W. Huang, C. Y. Liao, A. Q. Liu, N. I. Zheludev, G. Sun, and D. P. Tsai, Plasmon coupling in vertical split-ring resonator metamolecules, *Sci. Rep.* **5**, 9726 (2015).
- [14] S.-H. Gong, J.-H. Kim, Y.-H. Ko, C. Rodriguez, J. Shin, Y.-H. Lee, L. S. Dang, X. Zhang, and Y.-H. Cho, Self-aligned deterministic coupling of single quantum emitter to nano-focused plasmonic modes, *Proc. Natl. Acad. Sci., USA* **112**, 5280 (2015).
- [15] S. I. Azzam, K. Parto, and G. Moody, Purcell enhancement and polarization control of single-photon emitters in monolayer WSe₂ using dielectric nanoantennas, *Nanophotonics* **12**, 477 (2023).
- [16] Y. Kan and S. I. Bozhevolnyi, Advances in metaphotonics empowered single photon emission, *Adv. Opt. Mater.* **11**, 2202759 (2023).
- [17] J.-Y. Zhou, Q. Li, Z.-H. Hao, W.-X. Lin, Z.-X. He, R.-J. Liang, L. Guo, H. Li, L. You, J.-S. Tang, J.-S. Xu, C.-F. Li, and G.-C. Guo, Plasmonic-enhanced bright single spin defects in silicon carbide membranes, *Nano Lett.* **23**, 4334 (2023).
- [18] H. P. Adl, S. Gorji, M. K. Habil, I. Suárez, V. S. Chirvony, A. F. Gualdrón-Reyes, I. Mora-Seró, L. M. Valencia, M. de la Mata, J. Hernández-Saz, S. I. Molina, C. J. Zapata-Rodríguez, and J. P. Martínez-Pastor, Purcell enhancement and wavelength shift of emitted light by CsPbI₃ perovskite nanocrystals coupled to hyperbolic metamaterials, *ACS Photonics* **7**, 3152 (2020).
- [19] P. Zheng, L. Liang, S. Arora, K. Ray, S. Semancik, and I. Barman, Pyramidal hyperbolic metasurfaces enhance spontaneous emission of nitrogen-vacancy centers in nanodiamond, *Adv. Opt. Mater.* **11**, 2202548 (2023).
- [20] V. S. C. Manga Rao and S. Hughes, Single quantum dot spontaneous emission in a finite-size photonic crystal waveguide: Proposal for an efficient “on chip” single photon gun, *Phys. Rev. Lett.* **99**, 193901 (2007).
- [21] K. Hennessy, A. Badolato, M. Winger, D. Gerace, M. Atatüre, S. Gulde, S. Fält, E. L. Hu, and A. Imamoglu, Quantum nature of a strongly coupled single quantum dot–cavity system, *Nature (London)* **445**, 896 (2007).
- [22] D. O. Bracher, X. Zhang, and E. L. Hu, Selective Purcell enhancement of two closely linked zero-phonon transitions of a silicon carbide color center, *Proc. Natl. Acad. Sci. USA* **114**, 4060 (2017).
- [23] S. B. Hasan, A. P. Mosk, W. L. Vos, and A. Lagendijk, Finite-size scaling of the density of states in photonic band gap crystals, *Phys. Rev. Lett.* **120**, 237402 (2018).
- [24] F. Riboli, N. Caselli, S. Vignolini, F. Intonti, K. Vynck, P. Barthelemy, A. Gerardino, L. Balet, L. H. Li, A. Fiore, M. Gurioli, and D. S. Wiersma, Engineering of light confinement in strongly scattering disordered media, *Nat. Mater.* **13**, 720 (2014).
- [25] E. R. Martins, J. Li, Y. Liu, V. Depauw, Z. Chen, J. Zhou, and T. F. Krauss, Deterministic quasi-random nanostructures for photon control, *Nat. Commun.* **4**, 2665 (2013).
- [26] K. Vynck, M. Burreli, F. Riboli, and D. S. Wiersma, Photon management in two-dimensional disordered media, *Nat. Mater.* **11**, 1017 (2012).
- [27] L. Sapienza, H. Thyrestrup, S. Stobbe, P. D. Garcia, S. Smolka, and P. Lodahl, Cavity quantum electrodynamics with Anderson-localized modes, *Science* **327**, 1352 (2010).
- [28] N. Granchi, R. Spalding, M. Lodde, M. Petruzzella, F. W. Otten, A. Fiore, F. Intonti, R. Sapienza, M. Florescu, and M. Gurioli, Near-field investigation of luminescent hyperuniform disordered materials, *Adv. Opt. Mater.* **10**, 2102565 (2022).
- [29] N. Granchi, M. Lodde, K. Stokkerei, R. Spalding, P. J. van Veldhoven, R. Sapienza, A. Fiore, M. Gurioli, M. Florescu, and F. Intonti, Near-field imaging of optical nanocavities in hyperuniform disordered materials, *Phys. Rev. B* **107**, 064204 (2023).
- [30] P. D. García and P. Lodahl, Physics of quantum light emitters in disordered photonic nanostructures, *Ann. Phys.* **529**, 1600351 (2017).
- [31] S. K. Saini and R. V. Nair, Selective-frequency-gap-induced negative anisotropic scattering in designer photonic structures with short-range order, *Phys. Rev. A* **102**, 033529 (2020).
- [32] S. Yu, C.-W. Qiu, Y. Chong, S. Torquato, and N. Park, Engineered disorder in photonics, *Nat. Rev. Mater.* **6**, 226 (2021).
- [33] P. Mao, C. Liu, F. Song, M. Han, S. A. Maier, and S. Zhang, Manipulating disordered plasmonic systems by external cavity with transition from broadband absorption to reconfigurable reflection, *Nat. Commun.* **11**, 1538 (2020).
- [34] J. J. D. Leon, A. M. Hiszpanski, T. C. Bond, and J. D. Kuntz, Design rules for tailoring antireflection properties of hierarchical optical structures, *Adv. Opt. Mater.* **5**, 1700080 (2017).

- [35] M. D. Birowosuto, S. E. Skipetrov, W. L. Vos, and A. P. Mosk, Observation of spatial fluctuations of the local density of states in random photonic media, *Phys. Rev. Lett.* **105**, 013904 (2010).
- [36] B. Dieng, M. Beye, M. Toure, D. Diouf, D. Kobor, and A. S. Maiga, Design and optimization of silicon nanostructures, *OAJ Mater. Devices* **4**, 1 (2019).
- [37] L. Hong, Rusli, X. Wang, H. Zheng, H. Wang, X. Xiaoyan, and H. Yu, Light trapping in hybrid nanopyramid and nanohole structure silicon solar cell beyond the Lambertian limit, *J. Appl. Phys.* **116**, 074310 (2014).
- [38] Y. Wang, L. Yang, Y. Liu, Z. Mei, W. Chen, J. Li, H. Liang, A. Kuznetsov, and D. Xiaolong, Maskless inverted pyramid texturization of silicon, *Sci. Rep.* **5**, 10843 (2015).
- [39] M. Aalizadeh, M. R. Tavakol, A. Khavasi, M. Yilmaz, and E. Ozbay, Electromagnetic field tapering in the high-roughness substrates coated by a thin film of manganese: A lithography-free approach to ultra-broadband, wide-angle, UV to FIR perfect absorption, [arXiv:1812.01987](https://arxiv.org/abs/1812.01987).
- [40] Shinki, J. Singh, and S. Sarkar, Tuning the topographical parameters of Si pyramids for a better surface enhanced Raman response, *Phys. Chem. Chem. Phys.* **23**, 26407 (2021).
- [41] Shinki and S. Sarkar, Is 3D surface structuring always a prerequisite for effective SERS? *Surf. Interfaces* **33**, 102223 (2022).
- [42] K. X. Wang, Z. Yu, V. Liu, M. L. Brongersma, T. F. Jaramillo, and S. Fan, Nearly total solar absorption in ultrathin nanostructured iron oxide for efficient photoelectrochemical water splitting, *ACS Photonics* **1**, 235 (2014).
- [43] X. Wang, Z. Yang, P. Gao, X. Yang, S. Zhou, D. Wang, M. Liao, P. Liu, Z. Liu, S. Wu, J. Ye, and T. Yu, Improved optical absorption in visible wavelength range for silicon solar cells via texturing with nanopyramid arrays, *Opt. Express* **25**, 10464 (2017).
- [44] Sachchidanand and D. P. Samajdar, Performance enhancement of nanopyramid based Si hybrid solar cells utilizing the plasmonic properties of oxide coated metal nanoparticles, *Opt. Mater.* **107**, 110166 (2020).
- [45] A. Irmikimov, L. N. Paması, A. N. Hattori, T. Higashi, S. Takahashi, E. E. Hashamova, X. Shi, F. Guo, N. Hosoito, A. I. Osaka, H. Tanaka, and K. Hattori, Atomically architected silicon pyramid single-crystalline structure supporting epitaxial material growth and characteristic magnetism, *Crystal Growth Design* **21**, 946 (2021).
- [46] S. Zhong, W. Wang, Y. Zhuang, Z. Huang, and W. Shen, All-solution-processed random Si nanopyramids for excellent light trapping in ultrathin solar cells, *Adv. Funct. Mater.* **26**, 4768 (2016).
- [47] L. Yu, M. Batmunkh, M. Dadkhah, C. J. Shearer, and J. G. Shapter, Pyramid-textured antireflective silicon surface in graphene oxide/single-wall carbon nanotube-silicon heterojunction solar cells, *Energy Environ. Mater.* **1**, 232 (2018).
- [48] S. K. Saini, M. Halder, Y. Singh, and R. V. Nair, Bactericidal characteristics of bioinspired nontoxic and chemically stable disordered silicon nanopyramids, *ACS Biomater. Sci. Eng.* **6**, 2778 (2020).
- [49] E. Yablonovitch, Statistical ray optics, *J. Opt. Soc. Am.* **72**, 899 (1982).
- [50] E. D. Palik, *Handbook of Optical Constants of Solids* (Academic, New York, 1998), Vol. 3.
- [51] See Supplemental Material at <http://link.aps.org/supplemental/10.1103/PhysRevA.110.023522> for the details of FDTD simulation and optimization of random pyramids cavities; sample fabrication methodologies and scanning electron microscope images of samples as a function fill fraction; confocal imaging experiments and details of time-resolved measurements along with spatial-dependent focussing of excitation beam (see also reference [1] therein).
- [52] T. E. Scheul, E. Khorani, T. Rahman, M. D. B. Charlton, and S. A. Boden, Wavelength and angle resolved reflectance measurements of pyramidal textures for crystalline silicon photovoltaics, *Prog. Photovoltaics: Res. Appl.* **28**, 1248 (2020).
- [53] M. Balezin, K. V. Baryshnikova, P. Kapitanova, and A. B. Evlyukhin, Electromagnetic properties of the Great Pyramid: First multipole resonances and energy concentration, *J. Appl. Phys.* **124**, 034903 (2018).
- [54] N. Singh and R. V. Nair, Purcell and collection efficiency enhancement of single NV-center emission coupled to an asymmetric tamm structure, *Adv. Quantum Technol.* **6**, 2200142 (2023).
- [55] D. Bouchet, M. Mivelle, J. Proust, B. Gallas, I. Ozerov, M. F. Garcia-Parajo, A. Gulinatti, I. Rech, Y. De Wilde, N. Bonod, V. Krachmalnicoff, and S. Bidault, Enhancement and inhibition of spontaneous photon emission by resonant silicon nanoantennas, *Phys. Rev. Appl.* **6**, 064016 (2016).
- [56] J. M. Haimerl, I. Ghosh, B. König, J. M. Lupton, and J. Vogelsang, Chemical photocatalysis with rhodamine 6G: Investigation of photoreduction by simultaneous fluorescence correlation spectroscopy and fluorescence lifetime measurements, *J. Phys. Chem. B* **122**, 10728 (2018).
- [57] Priya, O. Schops, U. Woggon, and R. V. Nair, Inhibited spontaneous emission using gaplike resonance in disordered photonic structures, *Phys. Rev. A* **98**, 043835 (2018).
- [58] R. Sapienza, P. Bondareff, R. Pierrat, B. Habert, R. Carminati, and N. F. van Hulst, Long-tail statistics of the purcell factor in disordered media driven by near-field interactions, *Phys. Rev. Lett.* **106**, 163902 (2011).
- [59] G. M. Akselrod, C. Argyropoulos, T. B. Hoang, C. Ciraci, C. Fang, J. Huang, D. R. Smith, and M. H. Mikkelsen, Probing the mechanisms of large Purcell enhancement in plasmonic nanoantennas, *Nat. Photonics* **8**, 835 (2014).
- [60] M. Caldarola, P. Albella, E. Cortés, M. Rahmani, T. Roschuk, G. Grinblat, R. F. Oulton, A. V. Bragas, and S. A. Maier, Non-plasmonic nanoantennas for surface enhanced spectroscopies with ultra-low heat conversion, *Nat. Commun.* **6**, 7915 (2015).